Experimental Thermal and Fluid Science 73 (2016) 42–48

Contents lists available at ScienceDirect

Experimental Thermal and Fluid Science

journal homepage: www.elsevier.com/locate/etfs

Effect of burner diameter on the burning velocity of premixed turbulent flames stabilized on Bunsen-type burners

Parsa Tamadonfar *, Ömer L. Gülder

Institute for Aerospace Studies, University of Toronto, 4925 Dufferin Street, Toronto, Ontario M3H 5T6, Canada

ARTICLE INFO

Article history:
Received 31 August 2015
Received in revised form 5 September 2015
Accepted 6 September 2015
Available online 11 September 2015

Keywords:
Premixed turbulent flames
Flame height
Turbulent burning velocity

ABSTRACT

Influence of burner diameter on the turbulent burning velocity of premixed turbulent methane/air flames was studied on two Bunsen-type burners with nozzle inner diameters of 11.1 and 22.2 mm. The equivalence ratio was varied from 0.6 to 1.0. The non-dimensional turbulence intensity, non-dimensional bulk flow velocity, and non-dimensional longitudinal integral length scale were kept constant for a given equivalence ratio for both burners. Particle image velocimetry and Rayleigh scattering techniques were used to measure the instantaneous velocity and temperature fields, respectively. The characteristic flame height decreased with increasing equivalence ratio from 0.6 to 1.0 for both burners, whereas it increased considerably by increasing the burner diameter. The transverse profiles of the leading edge and half-burning surface flame surface densities showed a tall and narrow region at each side of the burner exit, whereas they were distributed over a larger area farther downstream of the burner exit. The leading edge and half-burning surface wrinkling factors were found to be higher for the larger burner farther downstream of the burner, whereas they are about the same near the burner exit. The non-dimensional leading edge turbulent burning velocity increased with increasing non-dimensional turbulence intensity for both burners. However, the leading edge turbulent burning velocity was found to be higher with the larger size burner.

© 2015 Elsevier Inc. All rights reserved.

1. Introduction

The development of low-emission combustion systems such as gas turbines for power generation and engines for transportation requires a better understanding of premixed turbulent combustion [1]. The detailed understanding of flame brush characteristics and turbulent burning velocity are highly desirable for the design of premixed combustion systems and numerical model testing [2].

In their comprehensive study of the turbulent burning velocity, S_T, Abdel-Gayed et al. [3] examined a large number of experimental data sets from Bunsen, spherical, and V-Shaped flames, and proposed a general correlation for the non-dimensional turbulent burning velocity, S_T/S_L^0, where S_L^0 is the unstrained premixed laminar burning velocity. This dimensionless correlation was generated by utilizing the turbulent burning velocities from various burner geometries, and it was in terms of the ratio of the effective root-mean-square (r.m.s.) of velocity fluctuations to the unstrained premixed laminar burning velocity, u'_k/S_L^0, and the Karlovitz flame stretch factor, Ka'. Bradley et al. [4] then showed that the ratio of S_T to u'_k has a power law relation to the product of the Karlovitz flame stretch factor, Ka', and the Lewis number, Le, by investigating the experimental data presented in [3]. Gülder [5] proposed conceptual models for the estimation of S_T for three combustion regimes. These models were tested by comparing them to the measured data of various experimental rigs covering the range from flames stabilized in ducts to expanding flames. It should be emphasized that all these models are in terms of the turbulence statistics, namely the total turbulence intensity and turbulent length scale. Lipatnikov and Chomiak [2] reviewed the available empirical correlations for the prediction of S_T in the literature, and discussed the effects of various parameters such as total turbulence intensity, u', longitudinal integral length scale, Λ_L, unstrained premixed laminar burning velocity, S_L^0, molecular heat diffusivity, κ, and pressure, P, on S_T.

In his review paper, Driscoll [6] argued that approaches based on the assumption that the real premixed turbulent flames should have the behavior of an ideal geometry-independent flame do not help to advance the field of premixed turbulent combustion. If this assumption were to be justified, the non-dimensional turbulent burning velocities for different flame geometries would be similar when the magnitudes of non-dimensional turbulence intensity, u'/S_L^0, non-dimensional longitudinal integral length scale, Λ_L/δ_f,

* Corresponding author.

http://dx.doi.org/10.1016/j.expthermflusci.2015.09.006
0894-1777/© 2015 Elsevier Inc. All rights reserved.

Nomenclature

Alphanumeric symbols

A_0	cross-sectional area of the burner (mm^2)
$A_{T,\langle c\rangle}$	mean turbulent flame surface area conditioned at a specific mean progress variable (mm^2)
c	progress variable
d	circular hole diameter of the turbulence generator (mm)
D	burner diameter for round Bunsen burner (mm)
Da	turbulent Damköhler number
f	focal length of the lens (mm)
h	axial distance from the burner exit (mm)
$H_{\langle c\rangle=0.5}$	characteristic flame height (mm)
I_R	intensity of the flame image
I_a	intensity of the air image
I_b	intensity of the background image
I	intensity ratio, see Eq. (2)
K	ratio of the fuel–air mixture Rayleigh scattering cross section to the pure-air Rayleigh scattering cross section, see Eq. (2)
Ka'	Karlovitz flame stretch factor
Ka	turbulent Karlovitz number
Le	Lewis number
M	mesh size of the turbulence generator (mm)
Ma_T	turbulent Markstein number
P	pressure
r	radial distance from the centerline of the burner (mm)
Re_{Λ_L}	turbulent Reynolds number
S_L^0	unstrained premixed laminar burning velocity (m/s)
S_T	turbulent burning velocity (m/s)
$S_{T,\langle c\rangle}$	turbulent burning velocity conditioned at a specific mean progress variable (m/s)
$S_{T,\langle c\rangle=0.05}$	leading edge turbulent burning velocity (m/s)
T_f	flame temperature (K)
T_a	air temperature (K)
T_{ad}	adiabatic flame temperature (K)
$\langle u^2\rangle^{1/2}$	root-mean-square of velocity fluctuations in the axial direction (m/s)
u'	total turbulence intensity (m/s)
u'_k	effective root-mean-square of velocity fluctuations (m/s)
U_B	bulk flow velocity (m/s)
$\langle v^2\rangle^{1/2}$	root-mean-square of velocity fluctuations in the radial direction (m/s)
$\langle w^2\rangle^{1/2}$	root-mean-square of velocity fluctuations in the azimuthal direction (m/s)
W	burner width for slot Bunsen burner (mm)

Greek symbols

$\alpha_{\langle c\rangle=0.05}$	power coefficient, see Eq. (5)
β	blockage ratio of the turbulence generator (mm)
χ_i	mole fraction of the ith species
δ_f	Zel'dovich thickness (mm)
η	Kolmogorov length scale (mm)
ϕ	equivalence ratio
κ	molecular heat diffusivity (m^2/s)
Λ_L	longitudinal integral length scale (mm)
ν	unburned mixture kinematic viscosity (m^2/s)
Ω_c	wrinkling factor
$\Omega_{c=0.05}$	leading edge wrinkling factor
$\Omega_{c=0.5}$	half-burning surface wrinkling factor
σ_m	fuel–air mixture Rayleigh scattering cross section (cm^2/sr)
σ_a	pure-air Rayleigh scattering cross section (cm^2/sr)
σ_i	Rayleigh scattering cross section of the ith species (cm^2/sr)
Σ	flame surface density (1/mm)
Σ_c	flame surface density conditioned at a specific progress variable (1/mm)
$\Sigma_{c=0.05}$	leading edge flame surface density (1/mm)
$\Sigma_{c=0.5}$	half-burning surface flame surface density (1/mm)
$\Xi_{\langle c\rangle=0.05}$	dimensionless number, see Eq. (5)

Others

Δs	interrogation box size (mm)
Δx	velocity vector spacing in the axial direction (mm)
$f(\Delta x)$	longitudinal velocity correlation coefficient

and the turbulent Markstein number, Ma_T, are equal, where the Zel'dovich thickness, δ_f, is the ratio of the reactant mass diffusivity to the unstrained premixed laminar burning velocity [1]. However, the real turbulent flames of each flame geometry are believed to have different values of S_T from other flame types under constant $u'/S_L^0, \Lambda_L/\delta_f$, and Ma_T due to the expectations that the wrinkling processes and boundary conditions would be different [6,7]. Hence, it is suggested that any correlations that are developed for one flame geometry should be specific to that geometry and should not be applicable for other flame types. Based on this recommendation, Filatyev et al. [8] suggested to include the bulk flow velocity, U_B, and burner width, W, as additional parameters in the turbulent burning velocity correlation of Bunsen-type flames since these parameters are believed to affect the wrinkling process and the resulting value of S_T. As a result, they proposed the following independent variables that influence the turbulent burning velocity [8]:

$$\frac{S_T}{S_L^0} = f\left(\frac{u'}{S_L^0}, \frac{\Lambda_L}{\delta_f}, Ma_T, \frac{U_B}{S_L^0}, \frac{W}{\delta_f}\right). \quad (1)$$

It is worth noting that in the turbulent burning velocity correlation suggested by Filatyev et al. [8], $\left(S_T - S_L^0\right)/S_L^0$ was proportional to $(W/\delta_f)^{1/2}$, although the burner width was not varied in the aforementioned experiments. Thus, the dependency of S_T on W was not proven. To the best of the authors' knowledge, there has not been any systematic investigation carried out on the effect of burner width (diameter) of the slot (round) Bunsen-type burner flames on the turbulent burning velocity when other parameters that are included in Eq. (1) are kept constant. Hence, the objective of this study was to determine the influence of Bunsen-type burner diameter on the turbulent burning velocity, and to assess whether the burner size should be included in empirical (or semi-empirical) correlations for the turbulent burning velocity of Bunsen-type flames.

2. Experimental methodology

The premixed turbulent flames were generated using two axisymmetric Bunsen-type burners with nozzle inner diameters of 11.1 and 22.2 mm. The filtered air and methane grade 2.0 flow rates were controlled using calibrated mass flow meters. A premixed ethylene/air pilot flame at the periphery of nozzle exit was utilized to attach the main flame to the rim of the burner. For each burner, the turbulence was generated by a passive turbulence generator mounted upstream of the burner exit. The turbulence generator holes are arranged in a hexagonal array.

Table 1
Summary of geometrical properties for turbulence generators.

D (mm)	d (mm)	M (mm)	β (%)
11.1	1.1	1.3	43
22.2	1.8	2.6	60

The circular hole diameter (d), mesh size (M), and blockage ratio (β) are the geometrical properties of the turbulence generator. Table 1 summarizes these properties of turbulence generators used in the current study. The small burner, $D = 11.1$ mm, has been previously used in this laboratory to study the structure of premixed turbulent flame fronts, see, for example, [9,10]. The details of the geometry for the small burner, $D = 11.1$ mm, and large burner, $D = 22.2$ mm, components were documented in [11,12], respectively.

Particle image velocimetry technique was utilized for characterization of turbulent flow fields. The light source was a double-pulsed Nd:YAG laser operating at an energy level and wavelength of 200 mJ/pulse and 532 nm, respectively. A LaVision light sheet optical assembly was used to convert the laser beam into a laser sheet. It consisted of two spherical lenses, $f = +85$ and -75 mm, and a cylindrical lens, $f = -20$ mm, where f is the focal length of the lens. This resulted in the formation of a laser sheet with a full-width-at-half-maximum (FWHM) of approximately 300 μm at the centerline of the burner. The seeding particles were produced by atomizing olive oil to sub-micron droplets by a nebulizer. A LaVision Imager pro X camera with a maximum resolution of 2048×2048 px^2 was utilized for recording the experimental images. The camera was equipped with a Sigma macro lens with a focal length of 105 mm operating at f/8.0. A 532 nm bandpass filter was mounted on the lens in order to reduce the interference of undesired wavelengths from the surrounding environment on the camera's CCD. The DaVis 7.2 software (FlowMaster, LaVision) was utilized to calculate the axial and radial velocity components. For each test condition, five hundred image pairs were obtained at a frequency of 6 Hz under the non-reacting condition. A multi-pass vector estimation technique was implemented on each image pair with interrogation box sizes decreasing from 64×64 to 32×32 px^2 with a 50% overlap. For all experimental conditions, the resolution and vector spacing were approximately 960 and 480 μm, respectively. The time delay between laser pulses was adjusted for each experimental condition to ensure that the displacement of seeding particles was less than a quarter of the final interrogation box size.

Two sets of experiments were performed in the current study. Conditions of these two sets are tabulated in Table 2. These conditions covered the regimes of corrugated flamelets and thin reaction zones as described in [1]. The equivalence ratio, ϕ, was varied from 0.6 to 1.0 for each set of experiments. The bulk flow velocity, U_B, was kept constant at 17.0 m/s for both sets of experiments. The total turbulence intensity and turbulent integral length scale are important parameters in the flame/flow interactions [13]. These statistics are controlled by the design and upstream location of the turbulence generator from the burner exit [13,14]. In this study, turbulence generators were inserted 89 and 44 mm upstream of the small and large burner exits, respectively. These positions were selected in order to keep the turbulence statistics constant for both burners. The root-mean-square (r.m.s.) of velocity fluctuations in the radial, $\langle v^2\rangle^{1/2}$, and azimuthal, $\langle w^2\rangle^{1/2}$, directions were assumed to be equal due to the axisymmetric nature of the flow field. Therefore, the velocity fluctuations in the axial, $\langle u^2\rangle^{1/2}$, and radial, $\langle v^2\rangle^{1/2}$, directions were utilized to estimate the total turbulence intensity from $u' = \sqrt{(\langle u^2\rangle + 2\langle v^2\rangle)/3}$. The longitudinal integral length scale, Λ_L, was obtained by integrating the longitudinal velocity correlation coefficient, $f(\Delta x)$, over the velocity vector spacing in the axial direction, Δx [15]. This integration was performed until the first location at which the longitudinal velocity correlation coefficient was equal to zero. The uncertainty associated with estimation of the longitudinal integral length scale was approximately 25%. These turbulence statistics, that is, u' and Λ_L, were averaged in a region between $-0.25 < r/D < 0.25$ and $0.1 < h/D < 0.5$ for each experimental condition, where r is the radial distance from the centerline of the burner, and h is the axial distance from the burner exit. The unstrained premixed laminar burning velocity, S_L^0, was evaluated using the Cantera package [16] with the GRI-Mech 3.0 mechanism [17]. The Zel'dovich thickness, δ_f, was determined by calculating the ratio of the reactant mass diffusivity to the unstrained premixed laminar burning velocity [1]. The non-dimensional bulk flow velocity, U_B/S_L^0, non-dimensional turbulence intensity, u'/S_L^0, and non-dimensional longitudinal integral length scale, Λ_L/δ_f, were almost constant at each equivalence ratio for both burners, see Table 2. The turbulent Reynolds, Karlovitz, and Damköhler numbers were estimated from $Re_{\Lambda_L} = u'\Lambda_L/\nu, Ka = (\delta_f/\eta)^2$, and $Da = \Lambda_L S_L^0/\delta_f u'$, respectively, where ν is the unburned mixture kinematic viscosity, and η is the Kolmogorov length scale calculated from $\eta = \Lambda_L Re_{\Lambda_L}^{-3/4}$.

The temperature fields of premixed turbulent flames were measured using the Rayleigh scattering technique. A single-pulsed Nd:YAG laser was utilized as a light source with a maximum energy and wavelength of 220 mJ/pulse and 355 nm, respectively. A UV-fused silica plano-concave lens, $f = -75$ mm, and a plano-convex lens, $f = +100$ mm, were used to focus the laser beam at the burner centerline. The focused beam was then converted into a laser sheet with a plano-concave cylindrical lens, $f = -25$ mm. This optical arrangement resulted in the formation of a laser sheet with a thickness of approximately 200 μm. An intensified CCD (ICCD) camera with a resolution of 1280×1024 px^2 was equipped with a Sodern-Cerco UV lens with a focal length and aperture size of 94 mm and f/4.1, respectively. A 355 nm bandpass filter was mounted on the lens to decrease the influence of unsought wavelengths from the surrounding environment on the camera's CCD. For each experimental condition, five hundred images were recorded at a frequency of 5 Hz using the DaVis 7.0 software (Rayleigh Thermometry, LaVision). A 3×3 px^2 non-linear sliding average filter was applied to reduce the noise on each raw image. The temperature field, $T_f(r,h)$, was then estimated using the following formula [18]:

$$T_f(r,h) = \frac{\sigma_m}{\sigma_a} T_a \frac{I_a - I_b}{I_R - I_b} = kT_a I, \tag{2}$$

where σ_m and σ_a are the fuel–air mixture and pure-air Rayleigh scattering cross sections, respectively. These parameters were evaluated from $\sigma_m = \left(\sum_i \sigma_i \chi_i\right)_m$ and $\sigma_a = \left(\sum_i \sigma_i \chi_i\right)_a$. The Rayleigh scattering cross section, σ_i, of the ith species was obtained from the results provided in [19]. The mole fraction of each species, χ_i, was evaluated by solving an adiabatic unstrained premixed laminar flame using the Cantera package [16]. T_a is the air temperature. I_R, I_a, and I_b are the intensity of the flame, reference, and background images, respectively. The reference image was recorded under the non-reacting condition by utilizing the co-flow in order to remove dust particles from the measurement area. The background intensity was estimated by solving Eq. (2) in the burned region by fixing $T_f = T_{ad}$, where T_{ad} is the adiabatic flame temperature [20]. The intensity ratio, I, showed a bimodal distribution for each experimental image. The peaks of the intensity ratio were associated with the unburned and burned temperatures [9]. In addition, a 4th order polynomial was established between the intensity ratio, I, and the

Table 2
Summary of experimental conditions.

Set of experiments	Flame	D (mm)	ϕ	U_B/S_L^0	u'/S_L^0	Λ_L/δ_f	Re_{Λ_L}	Ka	Da
I	A	11.1	0.6	144.1	6.5	11.7	103	7.8	1.8
	B	11.1	0.7	85.9	3.7	21.0	103	2.6	5.6
	C	11.1	0.8	60.9	2.7	28.5	103	1.3	10.7
	D	11.1	0.9	49.3	2.2	34.1	103	0.9	15.9
	E	11.1	1.0	44.0	2.0	40.2	103	0.7	20.1
II	F	22.2	0.6	144.1	5.5	12.7	104	4.2	2.3
	G	22.2	0.7	85.9	3.2	23.0	104	1.4	7.1
	H	22.2	0.8	60.9	2.3	31.6	104	0.7	13.5
	I	22.2	0.9	49.3	1.9	39.9	104	0.5	20.8
	J	22.2	1.0	44.0	1.7	48.3	104	0.4	27.8

ratio of the fuel–air mixture Rayleigh scattering cross section to the pure-air Rayleigh scattering cross section, k. Therefore, the R.H.S. of Eq. (2) was only dependent on a single parameter of I at a constant T_a. By performing these steps, the temperature field was estimated for each Rayleigh scattering image.

3. Results and discussion

3.1. Characteristic flame height

The characteristic flame height, $H_{\langle c\rangle=0.5}$, was considered as the vertical distance between the burner exit plane and the half-burning surface, $\langle c\rangle = 0.5$, along the flame centerline. Results show that the characteristic flame height decreased with increasing equivalence ratio from 0.6 to 1.0 for both burners, as shown in Fig. 1. This trend may be attributed to the increase of flame temperature resulting in the global reaction rate to increase. Similar observations were previously reported in the literature, see, for example, [14,21–23]. Moreover, increasing the burner diameter from 11.1 to 22.2 mm resulted in an increase in $H_{\langle c\rangle=0.5}$ between the range of 40% and 80% when the bulk flow velocity, total turbulence intensity, and longitudinal integral length scale were almost constant at each equivalence ratio for both burners.

3.2. Flame surface density and wrinkling factor

The flame surface density, Σ, characterizes the wrinkling of flame surface area with turbulence, and it can be estimated by calculating the mean flame surface area per unit volume [24,25]. In this study, the mean flame front perimeter per unit area was assumed to have the same trend as the mean flame surface area per unit volume. However, Bell et al. [26] showed that this assumption results in an underestimation of Σ by approximately 25–33% by performing direct numerical simulation (DNS) on a laboratory-scale turbulent slot flame of Filatyev et al. [8]. In this study, each of the progress variable image was divided into interrogation boxes with equal dimensions. The flame front perimeter in each interrogation box was estimated by multiplying the number of flame front pixels into the resolution of the image. The mean value of flame front perimeters for all captured images of one flame condition divided by the interrogation box area is then equal to Σ. A sensitivity analysis on the interrogation box size showed that increasing it from 0.56 to 2.32 mm does not have any significant effect on the magnitudes of $\Sigma_{c=0.5}$, where the subscript $c = 0.5$ indicates that the instantaneous flame front was selected at the half-burning surface for determination of Σ, Fig. 2. This observation implies that increasing the interrogation box size increases the probability of mean flame front perimeter presence in the larger area, whereas the ratio of the mean flame front perimeter to the interrogation box area does not change significantly.

The transverse profiles of the leading edge and half-burning surface flame surface densities, that is, $\Sigma_{c=0.05}$ and $\Sigma_{c=0.5}$, at various axial distances from the burner exit for Flame H are shown in Fig. 3 (a) and (b), respectively. The subscripts $c = 0.05$ and 0.5 indicate that the instantaneous flame fronts were selected at the leading edge and half-burning surface for determination of Σ, respectively. Near the burner exit, these profiles were tall and narrow at each side of the burner, whereas they became shorter and flame surfaces were distributed over a larger volume farther downstream of the burner exit. It is worth noting that the location of the

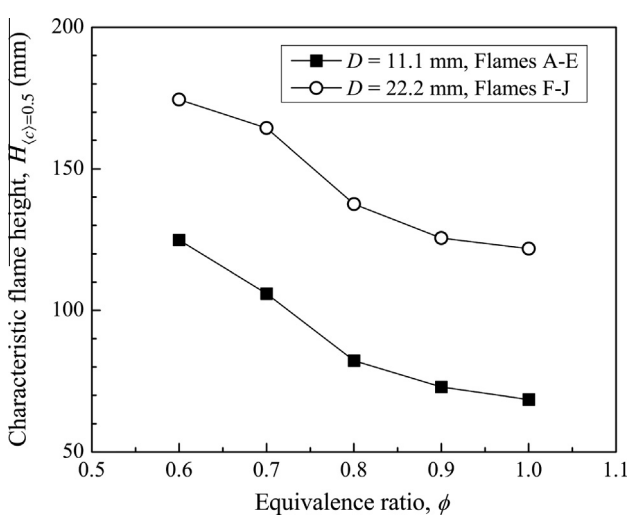

Fig. 1. Characteristic flame height with respect to the equivalence ratio for both burners.

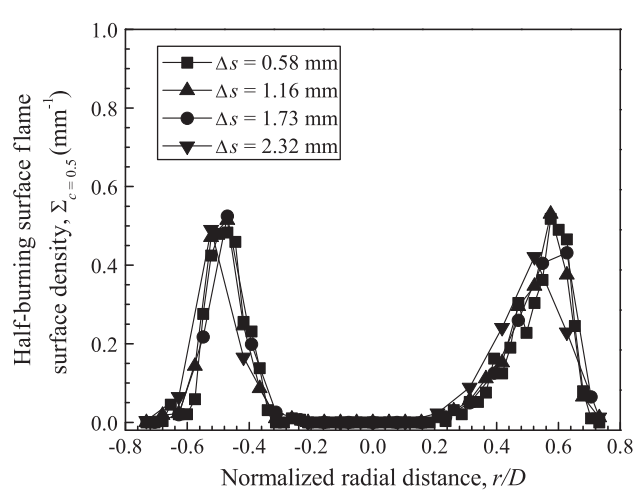

Fig. 2. Effect of the interrogation box size, Δs, on the transverse profile of the half-burning surface flame surface density, $\Sigma_{c=0.5}$, at $h/D = 2.5$ for Flame H.

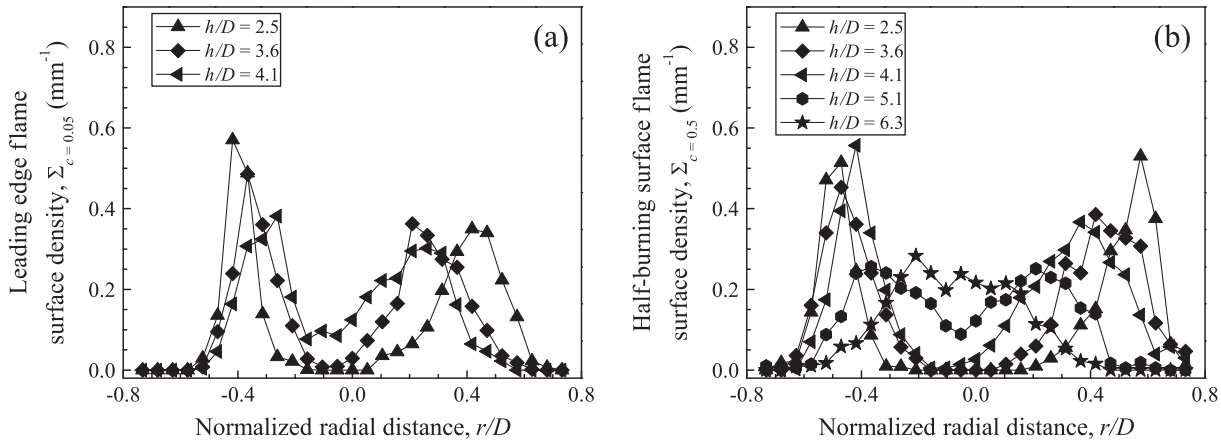

Fig. 3. Transverse profiles of (a) the leading edge flame surface density, $\Sigma_{c=0.05}$, and (b) the half-burning surface flame surface density, $\Sigma_{c=0.5}$, at various axial distances from the burner exit for Flame H. The interrogation box size, Δs, is equal to 1.16 mm.

maximum values of the leading edge and half-burning surface flame surface densities moved towards the centerline of the burner with increasing axial distance from the burner exit. Similar observations were previously reported for slot Bunsen flames, see, for example, [8,26,27], and for round Bunsen flames, see, for example, [28].

The degree of flame front wrinkling is the integral of flame surface density across the flame brush [8,29]. Therefore, the wrinkling factor conditioned at a specific progress variable, Ω_c, is defined by the following expression [8]:

$$\Omega_c = \frac{1}{2}\int_{-\infty}^{+\infty} \Sigma_c dr. \tag{3}$$

The leading edge and half-burning surface wrinkling factors, that is, $\Omega_{c=0.05}$ and $\Omega_{c=0.5}$, were calculated at various axial positions under the equivalence ratio of 0.8, as a representative condition, for each burner, as shown in Fig. 4(a) and (b). The half-burning surface wrinkling factor, $\Omega_{c=0.5}$, was larger than the leading edge wrinkling factor, $\Omega_{c=0.05}$, at a constant axial distance from the burner exit for each burner, indicating that the flame front wrinkling increases with increasing progress variable. Moreover, $\Omega_{c=0.05}$ and $\Omega_{c=0.5}$ were found to be higher for the larger burner, $D = 22.2$ mm, in comparison with corresponding values for the smaller burner, $D = 11.1$ mm. This observation suggests that increasing the burner diameter enhances the flame front wrinkling. The wrinkling factors were almost constant near the exit of both burners. This observation indicates that anchoring the main flame to the base of the burner restricts the flame front wrinkling. In addition, the wrinkling factor decreased considerably farther downstream of the burner exit. On the other hand, Filatyev et al. [8] showed that the wrinkling factor increases with increasing axial distance from the slot Bunsen burner exit, and Veynante et al. [30] reported that the flame front wrinkling is almost constant with increasing downstream position from the stabilizing rod of a V-Shaped flame.

3.3. Turbulent burning velocity

The turbulent burning velocity, $S_{T,\langle c\rangle}$, conditioned at a specific mean progress variable, $\langle c\rangle$, was evaluated using the following expression [6]:

$$S_{T,\langle c\rangle} = U_B \frac{A_0}{A_{T,\langle c\rangle}}, \tag{4}$$

where A_0 is the cross-sectional area of the burner exit, and $A_{T,\langle c\rangle}$ is the mean turbulent flame surface area conditioned at $\langle c\rangle$. The mean flame surface was constructed by rotating the two-dimensional mean flame front around the axial axis [14]. The choice of different $\langle c\rangle$ values for determining $A_{T,\langle c\rangle}$ is an arbitrary decision [6]. For example, Griebel et al. [14] used the contour of $\langle c\rangle = 0.05$, Zhang et al. [28] utilized the contour of $\langle c\rangle = 0.1$, and Venkateswaran [31] used the contour of $\langle c\rangle = 0.5$ for determining the mean turbulent flame surface area. In this study, the mean turbulent flame surface area was estimated by conditioning the mean progress variable at 0.05, and the corresponding burning velocity referred to as the leading edge turbulent burning velocity. The turbulence properties that affected the leading edge of the flame are strongly controlled by the turbulence characteristics given at the inlet of the burner. In addition, the turbulence statistics at the inlet of the burner are observed to be similar for both burners under constant equivalence ratio, see Table 2. Therefore, it is reasonable to investigate the effect of burner diameter on the leading edge turbulent burning velocity between these two burners.

The variations of the non-dimensional leading edge turbulent burning velocity with respect to the non-dimensional turbulence intensity are shown in Fig. 5. It is observed that the non-dimensional leading edge turbulent burning velocity increased with increasing non-dimensional turbulence intensity. Similar observations were previously reported in the literature, see, for example, [14,23,32]. If we compare the leading edge turbulent burning velocities, it is seen that the burning velocity increases with increasing equivalence ratio from 0.6 to 1.0. This increase may be due to an increase in the unstrained premixed laminar burning velocity. Most importantly, increasing the burner diameter by a factor of 2 resulted in an increase in $S_{T,\langle c\rangle=0.05}$ up to 13%. It seems that the flame front wrinkling for the larger burner, $D = 22.2$ mm, was larger than the corresponding value for the smaller burner, $D = 11.1$ mm. This increase may be the mechanism behind the increase of the leading edge turbulent burning velocity for the larger burner in comparison with corresponding value for the smaller burner. As shown in Table 2, the burner diameter was changed from 11.1 to 22.2 mm, whereas $U_B/S_L^0, u'/S_L^0$, and Λ_L/δ_f were almost constant at each equivalence ratio. Therefore, the following scaling is used to assess the effect of burner diameter on the burning velocity:

$$\Xi_{\langle c\rangle=0.05} = \frac{\left(S_{T,\langle c\rangle=0.05} - S_L^0\right)_{\phi,II}}{\left(S_{T,\langle c\rangle=0.05} - S_L^0\right)_{\phi,I}} = \left(\frac{D_{\phi,II}}{D_{\phi,I}}\right)^{\alpha_{\langle c\rangle=0.05}}, \tag{5}$$

where subscripts I and II refer to Flames A–E and F–J, respectively. It is observed that $\left(\left(S_{T,\langle c\rangle=0.05} - S_L^0\right)/S_L^0\right)_{\phi,II}$ varied linearly with respect to $\left(\left(S_{T,\langle c\rangle=0.05} - S_L^0\right)/S_L^0\right)_{\phi,I}$ with the slope of approximately 1.07, as

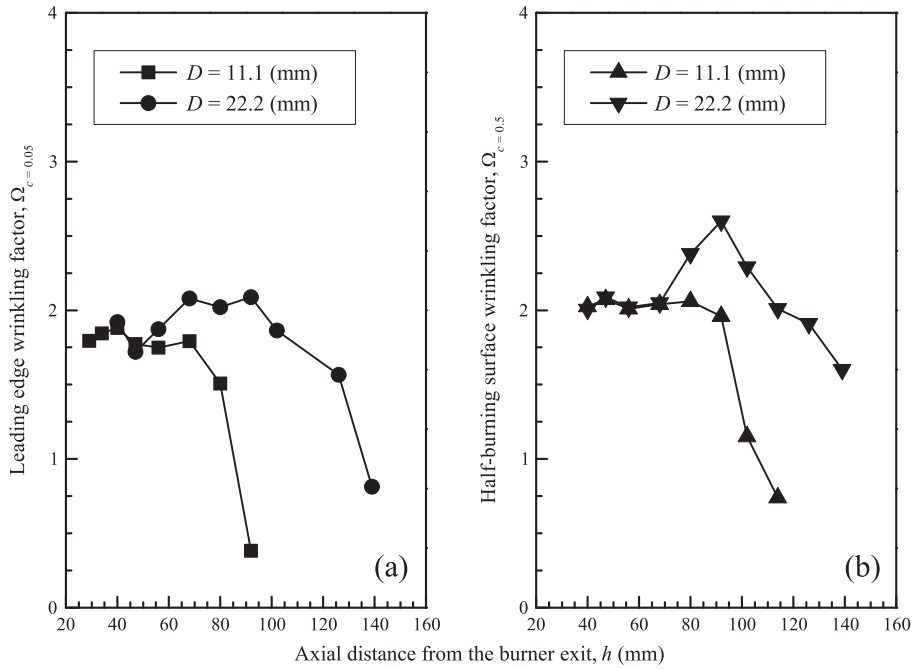

Fig. 4. (a) Leading edge and (b) half-burning surface wrinkling factors at various axial distances from the burner exit for Flames C and H.

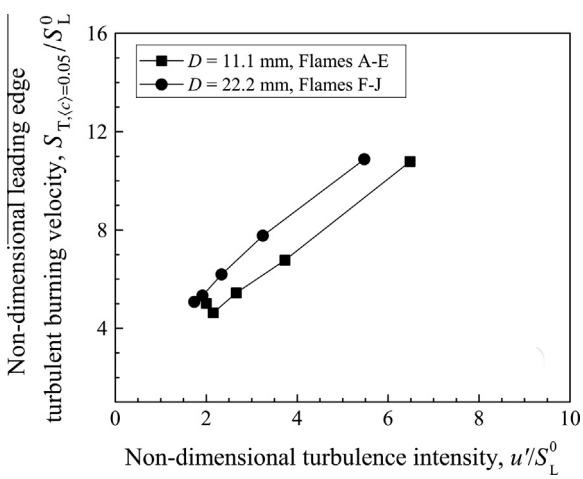

Fig. 5. Non-dimensional leading edge turbulent burning velocity with respect to the non-dimensional turbulence intensity for all operating conditions.

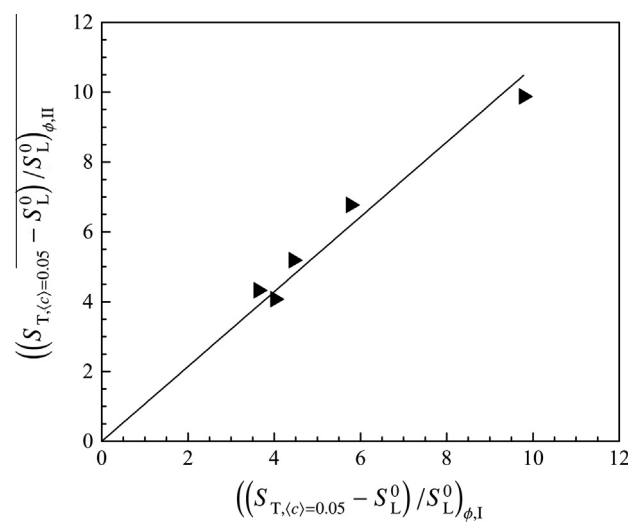

Fig. 6. Variation of $\left(\left(S_{T,\langle c\rangle=0.05}-S_L^0\right)/S_L^0\right)_{\phi,II}$ with respect to $\left(\left(S_{T,\langle c\rangle=0.05}-S_L^0\right)/S_L^0\right)_{\phi,I}$. Subscripts I and II refer to Flames A–E and F–J, respectively. Solid line is least-squares fit with the slope of approximately 1.07.

shown in Fig. 6. Therefore, the value of $\alpha_{\langle c\rangle=0.05}$ was estimated to be approximately 0.10.

The underlying physics of this result might be explained by the difference between residence times of the two burners. The residence time here refers to time available to wrinkle the flame and could be taken as the time it takes for a fluid parcel to travel from the burner rim to the measurement location. The flame sheets display similar wrinkling behavior close to the burner exit, but at a height of about 60 mm above the burner rim, the flame sheet of the larger burner displays more wrinkling than that of the smaller burner, Fig. 4. The larger burner with the same bulk flow velocity creates a longer flame height as compared to the smaller burner, as shown in Fig. 1. As a result, the flame sheet of the larger burner would have a longer residence time to wrinkle. The wider implication of this finding is that the empirical and semi-empirical formulations for turbulent burning velocity should include terms that account for the wrinkling residence time. Also, the variation, if any, of the observed residence time effect with turbulence parameters and with other flame geometries needs to be investigated.

4. Concluding remarks

The effect of burner diameter was investigated systematically on the turbulent burning velocity of premixed turbulent Bunsen flames. For this purpose, two burners with inner diameters of 11.1 and 22.2 mm were used. The equivalence ratio was increased from 0.6 to 1.0 for each burner. The non-dimensional turbulence intensity, bulk flow velocity, and longitudinal integral length scale were almost constant at each equivalence ratio for both burners.

The characteristic flame height decreased with increasing equivalence ratio from 0.6 to 1.0 for both burners, whereas it increased significantly by increasing the burner diameter.

The transverse profiles of the leading edge and half-burning surface flame surface densities showed a tall and narrow region at each side of the burner exit, whereas these profiles became wider farther downstream of the burner exit. The leading edge wrinkling factor was smaller than the half-burning surface wrinkling factor at a constant axial distance from the burner exit for each burner. These factors increased by increasing the burner diameter.

Results show that the non-dimensional leading edge turbulent burning velocity increased with increasing non-dimensional turbulence intensity for both burners. Furthermore, increasing the burner diameter by a factor of 2 resulted in the non-dimensional leading edge turbulent burning velocity to increase by about 10%.

Acknowledgments

The financial support from the Natural Sciences and Engineering Research Council of Canada through discovery (251116-2012) and strategic project (STPGP 430362-12) Grants awarded to the senior author is acknowledged.

References

[1] N. Peters, Turbulent Combustion, Cambridge University Press, 2000.
[2] A.N. Lipatnikov, J. Chomiak, Prog. Energy Combust. Sci. 28 (2002) 1–74.
[3] R.G. Abdel-Gayed, D. Bradley, M. Lawes, Proc. Roy. Soc. Lond. A 414 (1987) 389–413.
[4] D. Bradley, A.K.C. Lau, M. Lawes, Phil. Trans. Roy. Soc. Lond. A 338 (1992) 359–387.
[5] Ö.L. Gülder, Proc. Combust. Inst. 23 (1990) 743–750.
[6] J.F. Driscoll, Prog. Energy Combust. Sci. 34 (2008) 91–134.
[7] R.W. Bilger, S.B. Pope, K.N.C. Bray, J.F. Driscoll, Proc. Combust. Inst. 30 (2005) 21–42.
[8] S.A. Filatyev, J.F. Driscoll, C.D. Carter, J.M. Donbar, Combust. Flame 141 (2005) 1–21.
[9] F.T.C. Yuen, Ö.L. Gülder, AIAA J. 47 (2009) 2964–2973.
[10] F.T.C. Yuen, Ö.L. Gülder, Proc. Combust. Inst. 32 (2009) 1747–1754.
[11] F.T.C. Yuen, Experimental Investigation of the Dynamics and Structure of Lean-premixed Turbulent Combustion, Ph.D. thesis, University of Toronto Institute for Aerospace Studies, 2009.
[12] P. Tamadonfar, Ö.L. Gülder, Combust. Flame 162 (2015) 115–128.
[13] Y.C. Chen, R.W. Bilger, Exp. Therm. Fluid Sci. 27 (2003) 619–627.
[14] P. Griebel, P. Siewert, P. Jansohn, Proc. Combust. Inst. 31 (2007) 3083–3090.
[15] G.K. Batchelor, The Theory of Homogeneous Turbulence, Cambridge University Press, 1953.
[16] D. Goodwin, N. Malaya, H.K. Moffat, R. Speth, Cantera: An Object-oriented Software Toolkit for Chemical Kinetics, Thermodynamics, and Transport Processes. <http://code.google.com/p/cantera/>.
[17] G.P. Smith, D.M. Golden, M. Frenklach, N.W. Moriarty, B. Eiteneer, M. Goldenberg, C.T. Bowman, R.K. Hanson, S. Song, W.C. Gardiner, V.V. Lissianski, Z. Qin, GRI-Mech 3.0. <http://www.me.berkeley.edu/gri_mech/>.
[18] A. Soika, F. Dinkelacker, A. Leipertz, Proc. Combust. Inst. 27 (1998) 785–792.
[19] J.A. Sutton, J.F. Driscoll, Opt. Lett. 29 (2004) 2620–2622.
[20] D.A. Knaus, S.S. Sattler, F.C. Gouldin, Combust. Flame 141 (2005) 253–270.
[21] A. Boukhalfa, I. Gökalp, Combust. Flame 73 (1988) 75–87.
[22] B. Deschamps, Étude spatiale et temporelle de la structure dynamique et scalaire des flammes turbulentes premelangees de méthane–air, Ph.D. thesis, University of Orléans, 1990.
[23] P. Tamadonfar, Ö.L. Gülder, Combust. Flame 161 (2014) 3154–3165.
[24] I.G. Shepherd, R.K. Cheng, Combust. Flame 127 (2001) 2066–2075.
[25] Ö.L. Gülder, G.J. Smallwood, Combust. Sci. Technol. 179 (2007) 191–206.
[26] J.B. Bell, S.D. Marcus, J.F. Grcar, M.J. Lijewski, J.F. Driscoll, S.A. Filatyev, Proc. Combust. Inst. 31 (2007) 1299–1307.
[27] A.M. Steinberg, J.F. Driscoll, S.L. Ceccio, Exp. Fluids 44 (2008) 985–999.
[28] M. Zhang, J. Wang, J. Wu, Z. Wei, Z. Huang, H. Kobayashi, Int. J. Hydrogen Energy 39 (2014) 5176–5185.
[29] K.N.C. Bray, Proc. Roy. Soc. Lond. A 431 (1990) 315–335.
[30] D. Veynante, J. Piana, J.M. Duclos, C. Martel, Proc. Combust. Inst. 26 (1996) 413–420.
[31] P. Venkateswaran, Measurements and Modeling of Turbulent Consumption Speeds of Syngas Fuel Blends, Ph.D. thesis, Georgia Institute of Technology, 2013.
[32] F.T.C. Yuen, Ö.L. Gülder, Proc. Combust. Inst. 34 (2013) 1393–1400.